Carbon 109 (2016) 57–64

Contents lists available at ScienceDirect

Carbon

journal homepage: www.elsevier.com/locate/carbon

Reduced graphene oxide enhancing the photoelectrochemical properties of poly(3-hexylthiophene)

R. Gonçalves, F.C. Moraes, E.C. Pereira*

Department of Chemistry, Federal University of São Carlos, Mail Box 676, Postal Code 13565-905, São Carlos, SP, Brazil

ARTICLE INFO

Article history:
Received 13 May 2016
Received in revised form
30 June 2016
Accepted 18 July 2016
Available online 19 July 2016

ABSTRACT

Poly(3-hexylthiophene) has been used in different photoelectrochemical devices as active material. However, its efficiency regarding photo-conversion is low and the coupling with a second compound is necessary to reduce the electron-hole recombination effect on the generation of photocurrent. The low efficiency could be related to the organization of the polymer. In this work, we propose the use of reduced graphene oxide as modifier to P3HT to enhance its photocatalytic properties. The results here obtained strong suggest, both theoretically and experimentally, an important change in the polymer chain organization from twisted to planar configuration. As consequence, an important increase in the photoelectrochemical properties were observed. In the present case an improvement of over 50% in the value of the photocurrent comparing the pure material and the binary one, processed under the same conditions. In addition, the half-life of the charge carrier increased substantially from 0.781 ms to 9.54 ms. The results are promising because they demonstrate that a higher organization level of the polymer chains increases the photocatalytic properties of the material. Furthermore, the theoretical study not only explains why the properties are improved, but also leads to new understanding of the electronic structure obtained in a binary material.

1. Introduction

Conducting polymers have been receiving attention in the development of optoelectronic devices due to their low cost, environment-friendly features, mechanical flexibility, and high active area [1–3]; such properties make them suitable materials for organic photovoltaic (OPVs) solar cells [4–6]. Using the bulk-heterojunction (BHJ) concept [7,8], the photo-induced electron transfer from a conjugated polymer (donor) to an appropriate acceptor of electrons in OPVs can have a large donor/acceptor interface needed for the dissociation of the photo-generated excitons [9], minimizing the electron/hole recombination [10,11].

Among conducting polymers, polythiophene and its derivatives have been applied in different devices, such as capacitors [12], electrochromic displays [13], organic transistors [14], photoelectrochemical cells [15] and other optoelectronic devices [5]. Regarding optoelectronic devices, one of the most important materials is poly-3-hexylthiophene (P3HT) [16,17], generally used as the electron donor. Due to its hexyl ring-substituent, P3HT has superior processability and high degree of crystallinity [18]. In addition, this compound presents high hole mobility, environmental stability, and efficient light absorption in the visible range of the solar spectrum [17,19,20]. All these properties are highly dependent on the polymer chain organization and, then, they can be improved by increasing the π-stacking and the polymer regioregularity [21]. However, the synthesis of polymers with highly organized chains is not a trivial process and the presence of defects in the chains leads to high excitons recombination rates and slows down the charge transport [22]. Thus, in order to minimize the recombination rate and increase the charge transport one P3HT, it has been used a donor–acceptor copolymers or blends by incorporating electron-deficient and electron-rich building blocks in the same backbone.

Nanostructured carbon materials were evaluated to be used as electrons acceptors, among them fullerenes [8], particularly soluble C60 derivatives [1,23]. It was described that the photovoltaic characteristics of the composites (polymer/carbon material) have optimized properties; in particular enhanced optical absorption in the visible wavelength range, fast electron transfer and suitable

* Corresponding author.
E-mail address: ernesto@ufscar.br (E.C. Pereira).

http://dx.doi.org/10.1016/j.carbon.2016.07.041
0008-6223/

dielectric constant, resulting in good electron mobility. Although the record for the efficiency of OPVs has been obtained using polymer/fullerene devices [24,25], Nardes et al. [26] reported an improvement in the light absorption, and in consequence, in the photocurrent generation, which was achieved using self-organization of the individual components in a composite like BHJ. It was described that, in the case of fullerene derivatives and P3HT, the BHJ occurs only in the amorphous portion of the polymer [27]. Graphene is a smart material that can be used as a flat surface electron acceptor, it has been studied in several conversion and energy storage devices [28–30]. Due to its π-conjugated and two dimensional structure, graphene presents a set of properties that relates to the fact that its electrons behave as massless quantum particles [31]. In addition, graphene has high electron mobility at room temperature, good electronic, optical and phonon properties, as well as suitable thermal conductivity [19,32], making it an interesting material for application in solar cells [33]. Regarding the use of graphene as material to develop electrochemical devices, other interesting properties such as wide potential range, fast charge transfer, and electrocatalytic activity have been described in the literature [34]. In addition, it has an easily adaptable bandgap because of its reduced thickness of a few nanometer units [35].

Here we report a theoretical and experimental study of the conformational structure of P3HT after its interaction with reduced graphene oxide (rGO) and the effects of this interaction on its photoelectrochemical properties. The theoretical design is in agreement with experimental studies that demonstrated that the presence of rGO enhances the efficiency of photoconversion, reducing the recombination effect and creating a synergistic effect on the generation of photocurrent. Density Functional Theory (DFT) was employed to calculate the P3HT/rGO composite structure conformation; it is one of the most popular and versatile methods available in condensed matter physics and physical and computational chemistry. Because of its popularity, this theory finds applications in chemical and materials sciences for the interpretation and prediction of the behavior of complex systems in atomic scale. The application of this theory to conductive polymers is not new [36–40], it has been employed to estimate the properties of conductive polymers from the growth of its oligomers [38,39].

As polymers are very large systems, it is common to reduce the computational time by using a small representative fraction of the structural whole [41]. By using *ab initio* TDDFT [42] (time-dependent DFT), it is possible to calculate the excited states to understand the electronic properties of the donor-aceptor combination. It is also possible to develop a qualitative model for the charge transfer between the two materials. In this work, the proposed theoretical model was compared to experimental results in order to explain the observed changes in the system in a qualitative form.

2. Experimental

2.1. Chemicals and solutions

All chemicals were of analytical grade and were used without further purification. For polymer synthesis, 3-hexylthiophene monomer, chloroform, anhydrous iron (III) chloride, hydrochloric acid and EDTA were obtained from Sigma-Aldrich. The graphene oxide synthesis required graphite powder (<20 μ), sodium nitrate, sulfuric acid, nitric acid, potassium permanganate and hydrogen peroxide, all of them purchased from Sigma–Aldrich. For electrochemical measurements, acetonitrile, lithium perchlorate and perchloric acid used as the electrolyte were purchased from Sigma-Aldrich. All aqueous solutions were prepared with pure water from a Millipore Milli-Q system (resistivity closed to 18.2 MΩ cm).

2.2. P3HT and rGO synthesis

The P3HT synthesis has been extensively described in the literature [43–46]. Based on these reports, in this work, the polymer was obtained inside a drybox at 25 °C. A round-bottom flask with anhydrous chloroform solution containing $FeCl_3$, also anhydrous, and the monomer in the ratio of 4:1 was used. The polymerization reaction was carried out during 4 h with continuous stirring. After this, methanol was added to the system to stop the reaction and precipitate the polymer. The obtained powder was filtered through a sintered glass funnel, washed with methanol, acetone, HCl 10%, EDTA 10% and finally with ultra-pure water. After this step, the product was dried in an oven at 60 °C for 24 h.

Graphene oxide (GO) was prepared from graphite using a modified Hummer's method [47]. A mixture of graphite powder (10.0 g) and sodium nitrate (10.0 g) was treated with 400.0 mL of a concentrated solution of HNO_3/H_2SO_4 1:3 (volume) under magnetic stirring in an ice bath. Then, $KMnO_4$ (50.0 g) was slowly added and the mixture was left to react under vigorous stirring during 2 h. Subsequently, the temperature of the mixture was increased to 60 °C and the reaction was allowed to continue at this temperature under stirring for 30 additional minutes, before slowly adding 75.0 mL of H_2O_2 (30% $^{v}/_{v}$). Then, 100.0 mL of HCl solution (10% $^{v}/_{v}$) and 900.0 mL of purified water were added to the mixture, which was kept at 4 °C for 24 h. The light brownish supernatant was collected and the GO was separated, by centrifugation at 10,000 rpm in an Eppendorf 5804 centrifuge, and dried by lyophilization during 24 h.

The reduced graphene oxide (rGO) was prepared using a hydrothermal system assisted by microwave using 100.0 mg of GO and 80.0 mL of purified water. The mixture was submitted to the microwave-assisted hydrothermal treatment at 160 °C for 15 min. Due to the microwave hot spots, the GO was thermally reduced to rGO. The obtained rGO was separated by centrifugation at 10,000 rpm and dried by lyophilization during 24 h.

Two P3HT film samples were prepared by a casting method, one from a solution with the presence and the second in the absence of rGO. 18.0 mg of P3HT was dissolved in 1.0 mL of 1,2,3,4-tetrahydronaphthalene (tetralin) at 80 °C for 24 h with constant stirring. The samples containing reduced graphene oxide were obtained by adding 50% wt. of graphene and were later sonicated for 30 min. Then, a volume of 10 μL of each solution was deposited, each on a separate ITO substrate, and left to dry in vacuum desiccators for 12 h. A reduced graphene oxide film was used as a reference sample (blank). Indium-doped tin oxide (ITO) recovered glass with 10–15 Ω cm resistivity was used as substrate. Is important to notice that w ith this procedure we can obtain a fully dissolved P3HT added amount, on the other hand the solubility of rGO in tetralin is not complete, just part is dissolved, however the remain amount is totally dispersed and still stable for several days.

2.3. Apparatus and procedures

Cyclic voltammetry (CV) experiments were performed using a PGSTAT 302 Autolab electrochemical system (Eco Chemie, Netherlands) monitored with NOVA software. The special electrochemical cell, endowed with a quartz window, was assembled with a conventional three-electrode system: ITO plate modified with the composite (P3HT/rGO) as the working electrode, Ag/AgCl electrode in KCl solution (3.0 mol L^{-1}) as the reference electrode and a Pt wire as the auxiliary electrode. The CV measurements were recorded in acetonitrile/0.1 mol L^{-1} $LiClO_4$, in the potential range from 0.0 to +1.0 V, using a scan rate of 10 mV s^{-1}. Electrochemical impedance spectroscopy (EIS) data were obtained using a PC-controlled FRA2 (Eco Chemie, Netherlands), frequency response analyzer,

coupled to an Autolab potentiostat (model PGSTAT302, Eco Chemie, Netherlands). The frequency of the AC wave was scanned between 10 kHz and 10 mHz (10 data points per decade), with a 10 mV rms amplitude. All data were collected at open circuit potential. The measurements were carried out in 0.1 mol L^{-1} $HClO_4$ solution in two different conditions: dark and under illumination of a 250 W Xe lamp (100 mW cm^2). The impedance spectra were analyzed and the Randles equivalent circuit was used to fit the experimental results and determine the equivalent electrical parameter values for each experiment.

The morphological properties were determined by Scanning Electron Microscopy (SEM) using a FEI model Inspect F50. The spectroscopic characterization was made by Fourier transform infrared spectroscopy with attenuated total reflectance (ATR-FTIR) using a Bruker model Equinox 55 with samples in tetralin solution.

The time-dependent DFT theoretical study [42] (TD-DFT) was used to calculate the electronic properties of the system as well as the change in their geometries. A relaxation step was made using a semi-empirical method with PM7 basis in MOPAC2012 software. Then, geometrical optimizations were performed at Hartree-Fock level by using the HF-3c geometrical Counterpoise (gCP) correction [48] for dispersive interactions. All ground state DFT calculations were performed in tetralin solvent, using the COSMO solvation model [49], with the 3-21G [50,51] and 6-31G [52] basis sets. The ORCA [53] 3.0.3 software package was used for all HF/DFT geometry optimizations and the Gabedit software was used to visualize the molecular orbitals of the systems.

The initial model built for geometry optimization was designed based on the most likely possible interaction between the graphene sheet and the oligomeric chain. Then, the oligomer of P3HT was built starting from the monomer already optimized near to the basal plane of graphene sheet, also previously optimized. After building the P3HT and the rGO together, the composite was optimized using HF-3c.

The dihedral angle sets the angle formed by two planes that have a same vertex and it was measured following the scheme presented in Fig. 1; the numeration was made from the tail to head direction. For the situation in which two sulphur atoms of adjacent aromatic rings are facing the same direction and are in the same plane than the two carbon atoms that bonds them, the value of this dihedral is 0°.In the opposite situation, in which both point to opposite directions, the dihedral will be 180°, as shown in Fig. 1 (top). In the case of the graphene sheet, the 'dihedrals' were determined in the edges, so that the curvature of the graphene plane over each edge matched the dihedral angle, which was defined by two carbon atoms present in the "edges" of the sheet. In the case of this work, the dihedral angle was used to describe how far the planes formed in the structure must be aligned.

3. Results and discussion

3.1. Electrochemical characterization

In Fig. 2, a typical voltammograms for P3HT (curve a) in non-aqueous solution is presented. A couple of redox processes observed; the peak at +0.80 V can be attributed to polymer oxidation and the reduction peak observed at +0.75 V can be

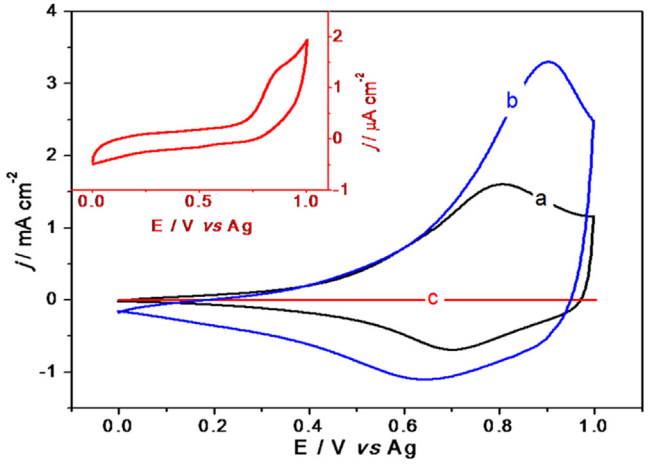

Fig. 2. Cyclic voltammetry experiments in ACN/$LiClO_4$ 0.1 mol L^{-1} with scan rate at 10 mV s^{-1}, for the following films: (a) P3HT; (b) P3HT/rGO; (c) rGO. (A colour version of this figure can be viewed online.)

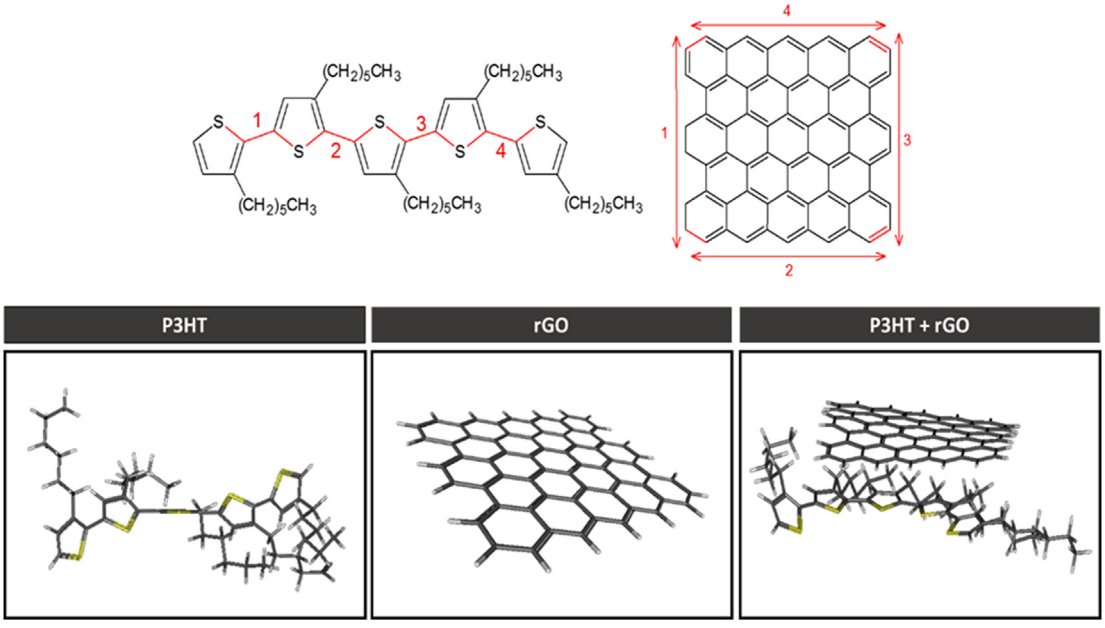

Fig. 1. Schematic representation of model construction for HF and DFT calculations. (A colour version of this figure can be viewed online.)

related to the reduction process. These redox process are recognized as P3HT fingerprints [54]. The composite material, P3HT/rGO (curve b) has also presented the P3HT reversible peaks, but in the oxidation process a shift of 95 mV towards more positive values is observed. Another important change is a 2-fold increase in the oxidation peak current. A surface area change or an electronic interaction between the rGO and P3HT could explain such change. The rGO film deposited on ITO was used as a blank (curve c); this blank only shows small electrochemical activity in the potential window investigated.

In order to elucidate the changes observed, a set of electrochemical impedance spectroscopy, EIS, experiments were carried out. The interpretation of EIS data allows the splitting and description of different parts of the system associated with both electronic and ionic transport. P3HT spectra were fitted using a modified Randles equivalent circuit, consisting of the cell resistance (R_{sol}) in series with a parallel combination of a constant phase element (*CPE*), considered as a pseudo-cacitance of the polymer (C_{mat}), and the resistance of the polymer, R_{pol}. In the case of the composite, it was necessary to add one more *RC* composition in parallel after the first, as can be observed in the Bode Plot presented in Fig. 3d. We have attributed these elements to the interaction between the two components of the composite and, therefore, they are here denominated as resistance and pseudo-capacitance of charge separation, R_{cs} and C_{cs}, respectively. We have associated this new process to the charge separation that occurs in the heterojunction interface. The time constant represented by the *CPE* can be considered as it appears at very high frequencies, i.e., as fast as expected for this kind of process.

Fig. 3a and b show the Nyquist plots for each compound in two conditions: presence and absence of the light source. A significant change is clearly observed for the semicircle size when the materials are under illumination, leading to the generation of photocurrent. The photocurrent magnitude provided by each material is related to the amount of excitons formed by illumination, which in turn can be understood as a drop in the resistance of the material due to light irradiation. Thereby, the resistance value for P3HT shows a decrease of 68.3%, and, for the composite, a decrease 75.0%, as expected. Another important difference is the polymer resistance values themselves. Under illumination, the composite resistance is of about 5.42 kΩ whereas P3HT alone has a value of 180 kΩ. This difference can be explained by two major factors: first the formation of the BHJ system. The P3HT has the behavior of a *p*-type semiconductor and the rGO of a *n*-type [28]. It is assumed that these characteristics promote a minimization in the electron/hole recombination facilitating the charge transfer. The interaction between the P3HT chains and the rGO sheets is a second factor to explain the observed changes. Since these are two aromatic molecules, a π-π stacking interaction is expected, which can bring an enhancement of the aromaticity in the system, leading to a conjugated system with fast charge transfer. In addition to this is the idea of an improvement in the charge carriers flow; comparing the capacitance values, it is observed 19.3 μF s^{n-1} cm^{-1} and only 8.82 μF s^{n-1} cm^{-1} for P3HT and P3HT/rGO, respectively. There is,

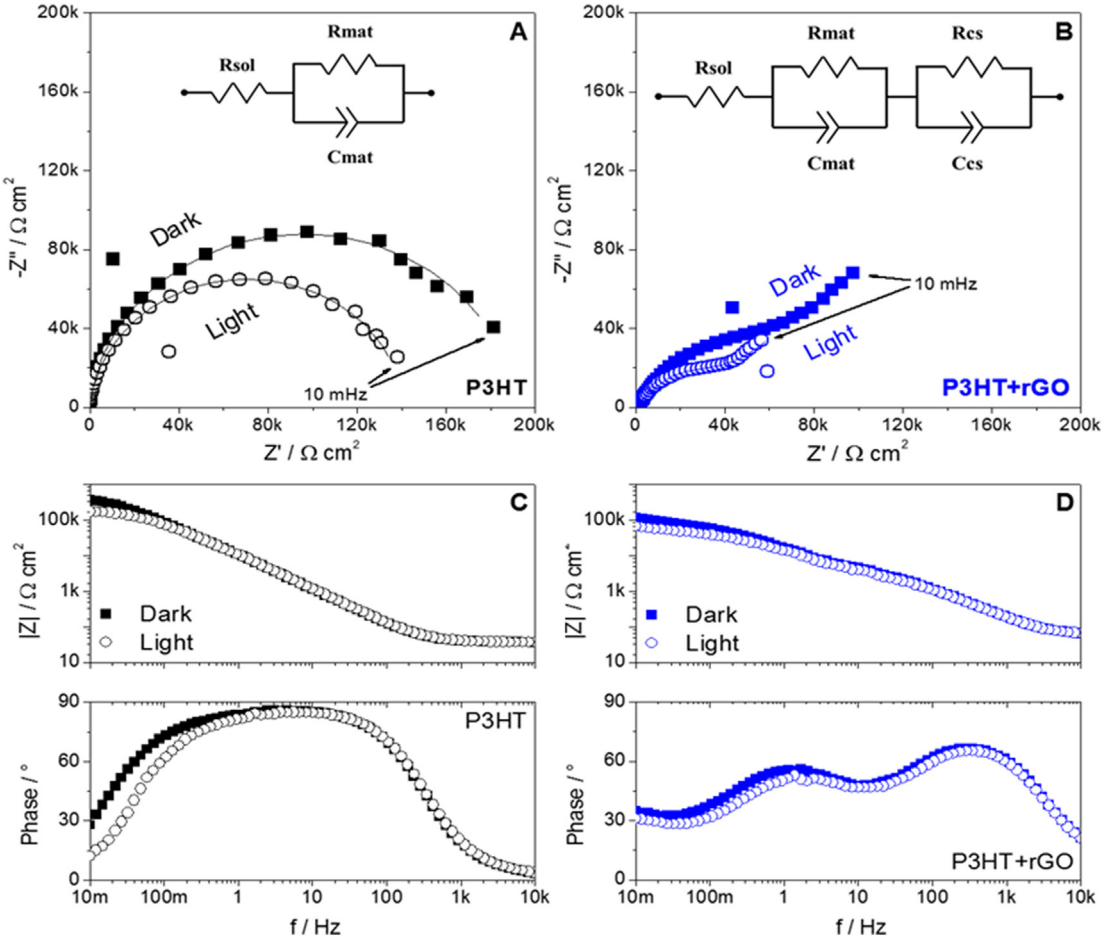

Fig. 3. Nyquist and Bode plots for P3HT and composite films. Frequency range from 10 kHz to 10 mHz, OCP *dc* potential, *ac* perturbation of 10 mV. (A colour version of this figure can be viewed online.)

therefore, a significant decrease in these pseudo-capacitances. Since this can be understood as the charge separation that occurs within the material due to the different mobility values for each charge carrier, an increase in the mobility of these carriers is a possible outcome.

The improvement in the electrochemical response could also be attributed to a morphology change, i.e., an increase in the electroactive area of the composite material could occur. Therefore, in Fig. 4, the morphologies of the materials are presented. A typical P3HT morphology consisting of a porous structure, described as sponge pattern [55], is observed. In Fig. 4b, it is observed that rGO is not present in a single layer structure and that there are overlaps of some layers. Also, it is clearly illustrated that rGO nanosheets are wrinkled and folded. Evaluating the image of the P3HT/rGO composite (Fig. 4c), it is possible to propose that P3HT covers the rGO sheets. Additionally, the surface becomes less porous and, then, is not expected that the change in the morphology is entirely responsible for the changes in the electrochemical behavior.

3.2. Theoretical structural study

In order to understand the interactions between the substances that lead to changes in the film properties, computational calculations were carried out using the HF/DFT method. As can be seen in the optimized structure forP3HT in Fig. 5 (bottom), the helicoidal structure is the lowest energy conformation for the polymer. In this case, *n* monomeric units in the chain are twisted by 54° when compared to the *n-1* monomer. This conformation occurs because of apolar hexyl substituents of the ring that tend to be directed towards the apolar solvent, while the sulphur atoms, which are polar, tend to be directed towards the inner portion of the structure [38]. The conformation of the graphene sheet, as expected, is extremely close to the plane, i.e. with dihedrals angles of less than 1°. Surprisingly, when the two materials interact by π-π stacking the optimized geometry presents planar P3HT chains, wherein the rings interacting with graphene now present a dihedral angle of about 7°, while the graphene is curved slightly as if in order to wrap the polymer chain.

In order to support the theoretical description above, ATR-FTIR experiments were carried out for P3HT, rGO and P3HT/rGO; the spectra are displayed in Fig. 5c. The important regions in the spectra are highlighted and it is possible to qualitatively compare the characteristic peaks attributed to P3HT and rGO. The first region appears in the range from 3100 to 2700 cm^{-1} with wagging-like vibration modes attributed to the sulphur atoms of the aromatic rings of P3HT. Also, the low intensity bands in this region could be attributed to the hybridized sp^2 carbon. This same behavior appeared in the rGO spectrum, for which there are no sulphur atoms expected in the structure. The second region, from 1700 to 600 cm^{-1}, has three important singular bands. These bands are related to C═C, S═O and C═O stretching. The coupling of the two highlighted regions in the spectra are due to stretching bands and can be described, for the P3HT spectrum, as out of plane twisting modes of the aromatic rings. For the graphene sheet, the coupled vibration mode can be understood as an oscillating movement. In this sense, it is important to stress out the change observed when comparing the pure compound with the composite. In the latter case, it is only possible to compare the wavelength position for each of the vibrational modes presented, but it is not possible to compare their intensities because in the theoretical spectrum the band intensities are attributed considering all of the vibrational modes calculated for the system.

Analyzing the twisting movement of the aromatic rings for the P3HT and the P3HT/rGO composite, it is observed that the band intensity decreases for the composite, which could be attributed to the suppression of the movement amplitude due to the strong interaction between the polymer and graphene. As consequence, the oscillating movement for graphene changes to a new kind of vibrational mode, a clamping movement that promotes the wrapping of the polymeric chain. On the other hand, an increase of the aromaticity degree is clear; this occurs due to the strong π-π interaction that appears in the new material. Finally, comparing the experimental and theoretical spectra for the composite, it is possible to observe that all described vibration modes have appeared in the theoretical spectrum, indicating that the new composite was synthetized.

Fig. 5a and b show the Molecular Orbitals calculated from HF-3c structural optimization for the composite. The strong π-π stacking interaction can be proven by means of molecular orbitals calculated by HF-3c, in which the six M.O. below the HOMO (HOMO-6) and two M.O. above the LUMO (LUMO+2) have π-symmetry. In addition, in each one of them there is overlap of the lobes of equal signs for the structures of both graphene and the polymer. It is important to stress out that the molecular orbitals of the polymer found with all aligned lobes indicate an improvement in the aromaticity of the polymer, which could explain the observed changes in the electrochemical properties of the material. With the π-orbitals aligned, there is a direct path with minimal charge transfer resistance, so that the conduction of electrons across the polymeric chain is facilitated. In addition, there is also an improvement in the efficiency of charge separation, because the excitons created in one component can be separated in the interface as electron-hole pairs, which have a large half-life because the hole remains in the polymer and the electron is collected by graphene.

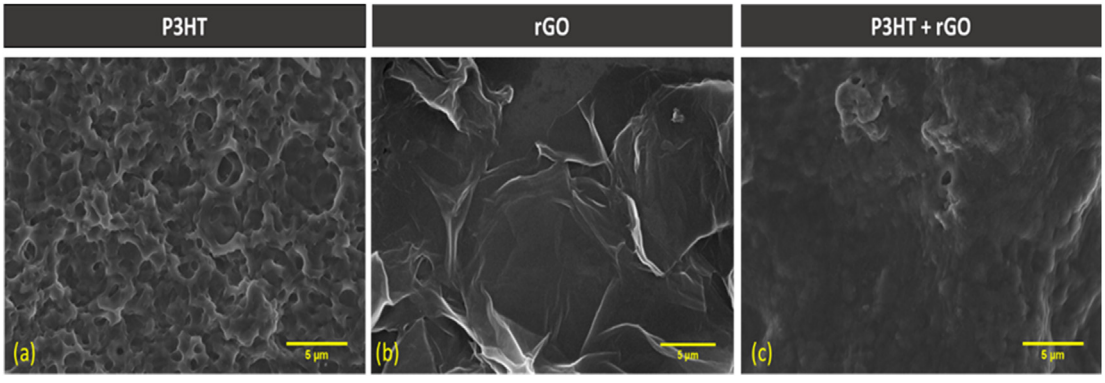

Fig. 4. FEG-SEM microscopy for each compound film in ITO substrate, 10 kx magnification and EHV level of 6 kV. (A colour version of this figure can be viewed online.)

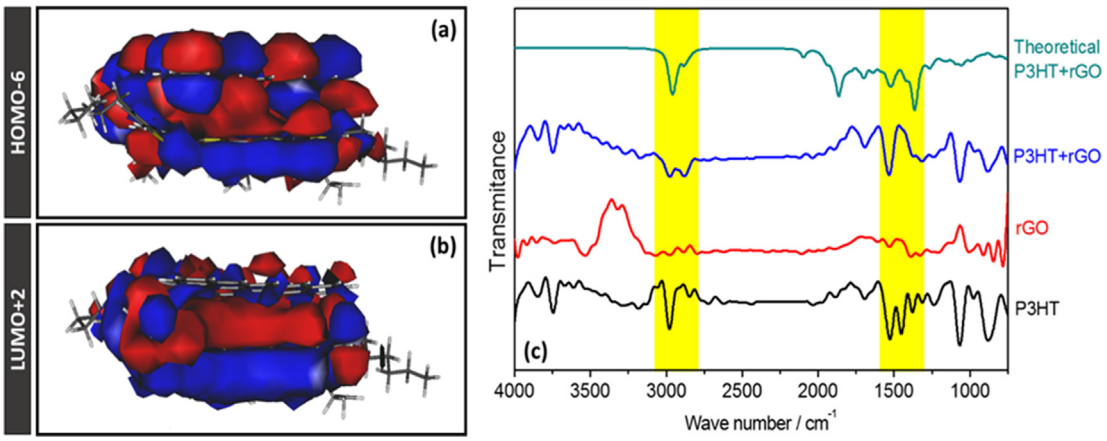

Fig. 5. Optimized HF-3c composite structure with its important Molecular Orbitals; and the experimental ATR-FTIR for compounds in tetralin solution compared to the vibrational spectrum of the composite. (A colour version of this figure can be viewed online.)

A different result from TDDFT calculations is the visualization of the electronic transitions in the molecular orbitals and, as consequence, it is possible to infer from which state the photogenerated charge is carried and to where it is transferred. Fig. 6a shows the transition molecular orbitals below and higher than the bandgap of the composite. These molecular orbitals have a main contribution from the graphene molecules, which can be explained by the band structure of this material [29,35]. Moreover, Fig. 6b and c show transitions involving both materials, the transitions shown are to the second and fifth excited states, respectively. This observation is very important because due to the interaction between the two materials, it is expected that the recombination effect will be less expressive.

Therefore, using impedance data it is possible to calculate the half-life for the charge carrier in each material following the Garcia-Belmont method [56,57]. Thus, for P3HT the life-time is 0.781 ms and for the composite it is 9.54 ms; so there is about 92% decrease in the number of combinations per second for the new material proposed. Moreover, even assuming that the thicknesses for the two films are almost equal, the mobility of the charge carriers further increases by about 10 times. We can attribute this observation to the strong interaction between these molecules that increase the aromaticity of the photoactive material, which is also a consequence of the π-π stacking interaction. Thus, it is expected that there will be an increase in the photocurrent obtained for the composite, since the recombination effect is a major problem with

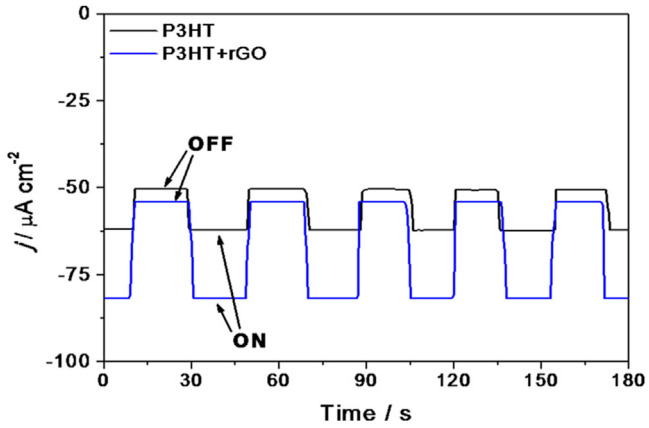

Fig. 7. Photocurrent response with time for P3HT (black line) and P3HT + rGO (blue line). 0.1 mol $L^{-1}HClO_4$, E = −0.6 V *versus* $Ag/AgCl/KCl_{3.0M}$. (A colour version of this figure can be viewed online.)

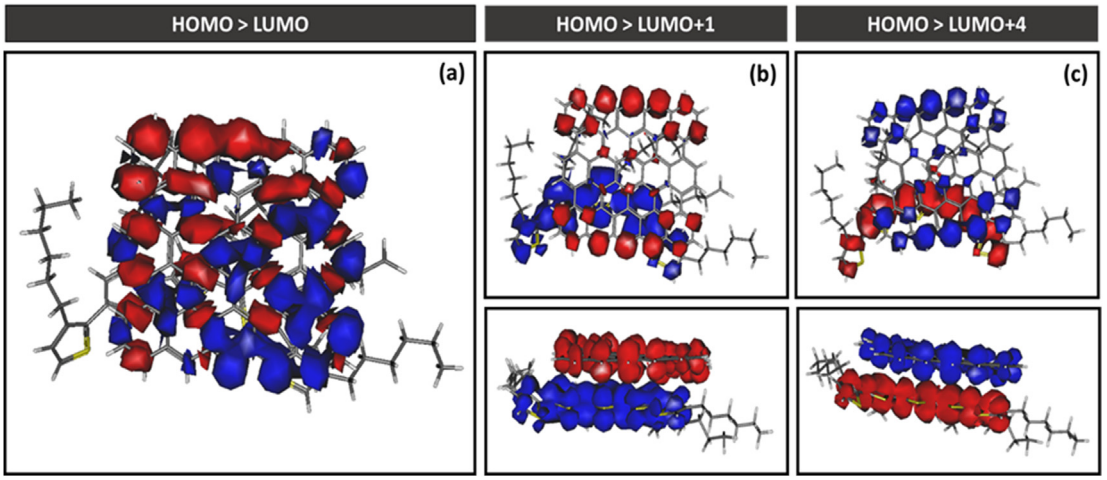

Fig. 6. Optimized HF-3c composite structure with its important transition Molecular Orbitals, the red ones represent the donor electronic density and the blue ones the acceptor states. (A colour version of this figure can be viewed online.)

this type of system.

Then, following the ideas described above, it was expected that the system containing the composite material should present a significant improvement in its photocurrent values. Fig. 7 shows the current response for the polymer and for the composite as a function of time. There is an increase of more than 2 times in the amount of photogenerated current.

This result is in agreement with the photo EIS, where the resistance value of the composite material is larger than that of P3HT. Moreover, the theoretical results show a strong interaction between the two molecules capable of changing the system morphology. In summary, two different mechanisms can explain the increase presented in Fig. 7: first, charge is generated in both materials because of the semiconductor properties of each one of them and, second, the charge is transferred in the BHJ interface created. These mechanisms benefit from better intermolecular interactions and increased interfacial area, which improve the heterojunction, promoted by the morphological changes observed for the studied material.

4. Conclusions

In this work, in which practical aspects were correlated with theoretical information, it was possible to understand which interactions exist between a semiconductor material of the *p*-type and another of the *n*-type when they form a bulk heterojunction. On one hand, by means of experimental characterization techniques, the intermolecular interactions were considered favorable for the macro properties of the material formed. A significant increase was observed in the electrochemical response, which led us to think that the polymeric chains were more accessible to the intercalation of ions and, thus, more easily passed to the oxidized state. On the other hand, also improving the electrochemical response as confirmed by electrochemical impedance measurements, the response to light excitation has also presented a significant gain. This type of response improvement was expected to be the consequence of an increase in the area; however, as confirmed by the SEM micrographs, the bulk film, which had morphology similar to that of a sponge, was flat and almost without pores. Thus, the system modeling contributed to show that the electronic interactions between graphene and the polymer chains change the way these are arranged in space, improving their properties at the molecular level; this fact reflects in their macroscopic properties. Moreover, it was possible to confirm the accuracy of the proposed model using the spectroscopic technique of ATR-FTIR and again, it was possible to have a broader view of what happens in the system in terms of suppression and displacement of bands.

Acknowledgments

Financial support from FAPESP 2013/07296-2, CNPq and CAPES is hereby gratefully acknowledged.

References

[1] M. Lanzi, E. Salatelli, T. Benelli, D. Caretti, L. Giorgini, F.P. Di-Nicola, A regioregular polythiophene-fullerene for polymeric solar cells, J. Appl. Polym. Sci. 132 (2015), http://dx.doi.org/10.1002/app.42121 n/a–n/a.
[2] F.C. Krebs, Fabrication and processing of polymer solar cells: a review of printing and coating techniques, Sol. Energy Mater. Sol. Cells. 93 (2009) 394–412, http://dx.doi.org/10.1016/j.solmat.2008.10.004.
[3] H. Spanggaard, F.C. Krebs, A brief history of the development of organic and polymeric photovoltaics, Sol. Energy Mater. Sol. Cells. 83 (2004) 125–146, http://dx.doi.org/10.1016/j.solmat.2004.02.021.
[4] A. Jannat, M.F. Rahman, M.S.H. Khan, A review study of organic photovoltaic cell, Int. J. Sci. Eng. Res. 4 (2013) 1–6. http://www.ijser.org/researchpaper%5CA-Review-Study-of-Organic-Photovoltaic-Cell.pdf.
[5] T.-P. Nguyen, Polymer-based nanocomposites for organic optoelectronic devices. A review, Surf. Coatings Technol. 206 (2011) 742–752, http://dx.doi.org/10.1016/j.surfcoat.2011.07.010.
[6] A.J. Heeger, Semiconducting polymers: the third generation, Chem. Soc. Rev. 39 (2010) 2354, http://dx.doi.org/10.1039/b914956m.
[7] A. Mishra, P. Bäuerle, Small molecule organic semiconductors on the move: promises for future solar energy technology, Angew. Chem. Int. Ed. 51 (2012) 2020–2067, http://dx.doi.org/10.1002/anie.201102326.
[8] J. Roncali, Molecular bulk heterojunctions: an emerging approach to organic solar cells, Acc. Chem. Res. 42 (2009) 1719–1730, http://dx.doi.org/10.1021/ar900041b.
[9] J.E. Coughlin, Z.B. Henson, G.C. Welch, G.C. Bazan, Design and synthesis of molecular donors for solution-processed high-efficiency organic solar cells, Acc. Chem. Res. 47 (2014) 257–270, http://dx.doi.org/10.1021/ar400136b.
[10] S.R. Cowan, N. Banerji, W.L. Leong, A.J. Heeger, Charge formation, recombination, and sweep-out dynamics in organic solar cells, Adv. Funct. Mater 22 (2012) 1116–1128, http://dx.doi.org/10.1002/adfm.201101632.
[11] A.J. Heeger, 25th anniversary article: bulk heterojunction solar cells: understanding the mechanism of operation, Adv. Mater 26 (2014) 10–28, http://dx.doi.org/10.1002/adma.201304373.
[12] A. Laforgue, P. Simon, C. Sarrazin, J.-F. Fauvarque, Polythiophene-based supercapacitors, J. Power Sources 80 (1999) 142–148, http://dx.doi.org/10.1016/S0378-7753(98)00258-4.
[13] M. Nicho, Synthesis of derivatives of polythiophene and their application in an electrochromic device, Sol. Energy Mater. Sol. Cells 82 (2004) 105–118, http://dx.doi.org/10.1016/j.solmat.2004.01.009.
[14] N.D. Treat, J.A. Nekuda Malik, O. Reid, L. Yu, C.G. Shuttle, G. Rumbles, et al., Microstructure formation in molecular and polymer semiconductors assisted by nucleation agents, Nat. Mater 12 (2013) 628–633, http://dx.doi.org/10.1038/nmat3655.
[15] H.-J. Wang, C.-P. Chen, R.-J. Jeng, Polythiophenes comprising conjugated pendants for polymer solar cells: a review, Mater. (Basel) 7 (2014) 2411–2439, http://dx.doi.org/10.3390/ma7042411.
[16] A. Facchetti, Polymer donor–polymer acceptor (all-polymer) solar cells, Mater. Today 16 (2013) 123–132, http://dx.doi.org/10.1016/j.mattod.2013.04.005.
[17] A. Marrocchi, D. Lanari, A. Facchetti, L. Vaccaro, Poly(3-hexylthiophene): synthetic methodologies and properties in bulk heterojunction solar cells, Energy Environ. Sci. 5 (2012) 8457, http://dx.doi.org/10.1039/c2ee22129b.
[18] D. Kekuda, H.-S. Lin, M. Chyi Wu, J.-S. Huang, K.-C. Ho, C.-W. Chu, The effect of solvent induced crystallinity of polymer layer on poly(3-hexylthiophene)/C70 bilayer solar cells, Sol. Energy Mater. Sol. Cells 95 (2011) 419–422, http://dx.doi.org/10.1016/j.solmat.2010.05.055.
[19] R. Bkakri, A. Sayari, E. Shalaan, S. Wageh, A.A. Al-Ghamdi, A. Bouazizi, Effects of the graphene doping level on the optical and electrical properties of ITO/P3HT: graphene/Au organic solar cells, Superlattices Microstruct. 76 (2014) 461–471, http://dx.doi.org/10.1016/j.spmi.2014.10.016.
[20] C. Kang, S. Kim, Y. Hong, C. Lee, Frequency analysis on poly(3-hexylthiopene) rectifier using impedance spectroscopy, Thin Solid Films 518 (2009) 889–892, http://dx.doi.org/10.1016/j.tsf.2009.07.110.
[21] Y. Harima, X. Jiang, R. Patil, K. Komaguchi, H. Mizota, Influence of film structure on mobilities of charge carriers in conducting polymers, Electrochim. Acta 52 (2007) 8088–8095, http://dx.doi.org/10.1016/j.electacta.2007.07.007.
[22] P.P. Boix, J. Ajuria, I. Etxebarria, R. Pacios, G. Garcia-Belmonte, Kinetics of occupancy of defect states in poly(3-hexylthiophene):fullerene solar cells, Thin Solid Films 520 (2012) 2265–2268, http://dx.doi.org/10.1016/j.tsf.2011.09.044.
[23] G. Dennler, M.C. Scharber, C.J. Brabec, Polymer-fullerene bulk-heterojunction solar cells, Adv. Mater 21 (2009) 1323–1338, http://dx.doi.org/10.1002/adma.200801283.
[24] M.T. Dang, L. Hirsch, G. Wantz, P3HT: PCBM, best seller in polymer photovoltaic research, Adv. Mater 23 (2011) 3597–3602, http://dx.doi.org/10.1002/adma.201100792.
[25] M.A. Brady, G.M. Su, M.L. Chabinyc, Recent progress in the morphology of bulk heterojunction photovoltaics, Soft Matter 7 (2011) 11065, http://dx.doi.org/10.1039/c1sm06147j.
[26] A.M. Nardes, A.J. Ferguson, P. Wolfer, K. Gui, P.L. Burn, P. Meredith, et al., Free carrier generation in organic photovoltaic bulk heterojunctions of conjugated polymers with molecular acceptors: planar versus spherical acceptors, ChemPhysChem. 15 (2014) 1539–1549, http://dx.doi.org/10.1002/cphc.201301022.
[27] J.M. Lobez, T.L. Andrew, V. Bulović, T.M. Swager, Improving the performance of P3HT–Fullerene solar cells with side-chain-functionalized poly(thiophene) additives: a new paradigm for polymer design, ACS Nano 6 (2012) 3044–3056, http://dx.doi.org/10.1021/nn204589u.
[28] D. Chen, H. Zhang, Y. Liu, J. Li, Graphene and its derivatives for the development of solar cells, photoelectrochemical, and photocatalytic applications, Energy Environ. Sci. 6 (2013) 1362, http://dx.doi.org/10.1039/c3ee23586f.
[29] F. Bonaccorso, Z. Sun, T. Hasan, A.C. Ferrari, Graphene photonics and optoelectronics, Nat. Photonics 4 (2010) 611–622, http://dx.doi.org/10.1038/nphoton.2010.186.
[30] L. Grande, V.T. Chundi, D. Wei, C. Bower, P. Andrew, T. Ryhänen, Graphene for energy harvesting/storage devices and printed electronics, Particuology 10

(2012) 1–8, http://dx.doi.org/10.1016/j.partic.2011.12.001.
[31] A. Krishnan, E. Dujardin, M.M.J. Treacy, J. Hugdahl, S. Lynum, T.W. Ebbesen, Graphitic cones and the nucleation of curved carbon surfaces, Nature 388 (1997) 451–454.
[32] V. Singh, D. Joung, L. Zhai, S. Das, S.I. Khondaker, S. Seal, Graphene based materials: past, present and future, Prog. Mater. Sci. 56 (2011) 1178–1271, http://dx.doi.org/10.1016/j.pmatsci.2011.03.003.
[33] J.D. Roy-Mayhew, D.J. Bozym, C. Punckt, I.A. Aksay, Functionalized graphene as a catalytic counter electrode in dye-sensitized solar cells, ACS Nano 4 (2010) 6203–6211, http://dx.doi.org/10.1021/nn1016428.
[34] F.C. Moraes, R.G. Freitas, R. Pereira, L.F. Gorup, A. Cuesta, E.C. Pereira, Coupled electronic and morphologic changes in graphene oxide upon electrochemical reduction, Carbon N. Y. 91 (2015) 11–19, http://dx.doi.org/10.1016/j.carbon.2015.04.038.
[35] Y. Zhang, T.-T. Tang, C. Girit, Z. Hao, M.C. Martin, A. Zettl, et al., Direct observation of a widely tunable bandgap in bilayer graphene, Nature 459 (2009) 820–823, http://dx.doi.org/10.1038/nature08105.
[36] J. Smith, P. Cox, N.M. Ratcliffe, S. Campbell, Conducting polymers as coatings: electrochemical and density functional theory investigations of the polymerisation, Trans. Inst. Metal. Finish. (2002). http://eprints.uwe.ac.uk/19765/ (accessed 17.07.15).
[37] A. Ehsani, F. Babaei, H. Mostaanzadeh, Electrochemical and optical investigation of conductive polymer and MWCNT nanocomposite film, J. Braz. Chem. Soc. 26 (2014) 331–337, http://dx.doi.org/10.5935/0103-5053.20140284.
[38] J.A. Schmidt, R.E. Koehn, T.M. Pappenfus, J.D. Alia, PBC-DFT: an Efficient Method to Calculate Energy Band Gaps of Conducting Polymers Used in Solar Cells, 2010. http://conservancy.umn.edu/handle/11299/101775 (accessed 17.07.15).
[39] S. Yang, P. Olishevski, M. Kertesz, Bandgap calculations for conjugated polymers, Synth. Met. 141 (2004) 171–177, http://dx.doi.org/10.1016/j.synthmet.2003.08.019.
[40] H. Shirani Il Beigi, S. Jameh-Bozorghi, Theoretical study on the electronic, structural, properties and reactivity of a series of mono-, di-, tri- and tetrachlorothiophenes as well as corresponding radical cation forms as monomers for conducting polymers, Chem. Cent. J. 5 (2011) 13, http://dx.doi.org/10.1186/1752-153X-5-13.
[41] J.P. Perdew, K.A. Jackson, M.R. Pederson, D.J. Singh, C. Fiolhais, Atoms, molecules, solids, and surfaces: applications of the generalized gradient approximation for exchange and correlation, Phys. Rev. B 46 (1992) 6671–6687, http://dx.doi.org/10.1103/PhysRevB.46.6671.
[42] E. Runge, E.K.U. Gross, Density-Functional theory for time-dependent systems, Phys. Rev. Lett. 52 (1984) 997–1000, http://dx.doi.org/10.1103/PhysRevLett.52.997.
[43] R.D. McCullough, R.D. Lowe, M. Jayaraman, D.L. Anderson, Design, synthesis, and control of conducting polymer architectures: structurally homogeneous poly(3-alkylthiophenes), J. Org. Chem. 58 (1993) 904–912, http://dx.doi.org/10.1021/jo00056a024.
[44] J.N. de Freitas, M.A. Mamo, M. Maubane, W.A.L. van Otterlo, N.J. Coville, A.F. Nogueira, Nanocomposites of gold and poly(3-hexylthiophene) containing fullerene moieties: synthesis, characterization and application in solar cells, J. Power Sources 215 (2012) 99–108, http://dx.doi.org/10.1016/j.jpowsour.2012.04.066.
[45] M.R. Karim, Synthesis and characterizations of poly(3-hexylthiophene) and modified carbon nanotube composites, J. Nanomater 2012 (2012) 1–8, http://dx.doi.org/10.1155/2012/174353.
[46] S. Amou, O. Haba, K. Shirato, T. Hayakawa, M. Ueda, K. Takeuchi, et al., Head-to-tail regioregularity of poly(3-hexylthiophene) in oxidative coupling polymerization with $FeCl_3$, J. Polym. Sci. Part A Polym. Chem. 37 (1999) 1943–1948, http://dx.doi.org/10.1002/(SICI)1099-0518(19990701)37:13<1943::AID-POLA7>3.0.CO;2-X.
[47] W.S. Hummers, R.E. Offeman, Preparation of graphitic oxide, J. Am. Chem. Soc. 80 (1958), http://dx.doi.org/10.1021/ja01539a017, 1339–1339.
[48] R. Sure, S. Grimme, Corrected small basis set Hartree-Fock method for large systems, J. Comput. Chem. 34 (2013) 1672–1685, http://dx.doi.org/10.1002/jcc.23317.
[49] S. Sinnecker, A. Rajendran, A. Klamt, M. Diedenhofen, F. Neese, Calculation of solvent shifts on electronic g-tensors with the conductor-like screening model (COSMO) and its self-consistent generalization to real solvents (direct COSMO-RS), J. Phys. Chem. A 110 (2006) 2235–2245, http://dx.doi.org/10.1021/jp056016z.
[50] T. Clark, J. Chandrasekhar, G.W. Spitznagel, P.V.R. Schleyer, Efficient diffuse function-augmented basis sets for anion calculations. III. The 3-21+G basis set for first-row elements, Li-F, J. Comput. Chem. 4 (1983) 294–301, http://dx.doi.org/10.1002/jcc.540040303.
[51] M.S. Gordon, J.S. Binkley, J.A. Pople, W.J. Pietro, W.J. Hehre, Self-consistent molecular-orbital methods. 22. Small split-valence basis sets for second-row elements, J. Am. Chem. Soc. 104 (1982) 2797–2803, http://dx.doi.org/10.1021/ja00374a017.
[52] W.J. Hehre, Self—Consistent molecular orbital methods. XII. Further extensions of Gaussian—Type basis sets for use in molecular orbital studies of organic molecules, J. Chem. Phys. 56 (1972) 2257, http://dx.doi.org/10.1063/1.1677527.
[53] F. Neese, The ORCA program system, Wiley Interdiscip. Rev. Comput. Mol. Sci. 2 (2012) 73–78, http://dx.doi.org/10.1002/wcms.81.
[54] R. Gonçalves, A.A. Correa, R. Pereira, E.C. Pereira, Investigation of the electrochemical aging of poly(3-hexiltiophene) using impedance spectroscopy, Electrochim. Acta 190 (2016) 329–336, http://dx.doi.org/10.1016/j.electacta.2015.12.198.
[55] K. Tremel, S. Ludwigs, Morphology of P3HT in thin films in relation to optical and electrical properties, Adv. Polym. Sci. (2014) 39–82, http://dx.doi.org/10.1007/12_2014_288.
[56] G. Garcia-Belmonte, A. Munar, E.M. Barea, J. Bisquert, I. Ugarte, R. Pacios, Charge carrier mobility and lifetime of organic bulk heterojunctions analyzed by impedance spectroscopy, Org. Electron. Phys. Mater. Appl. 9 (2008) 847–851, http://dx.doi.org/10.1016/j.orgel.2008.06.007.
[57] G. Garcia-Belmonte, P.P. Boix, J. Bisquert, M. Sessolo, H.J. Bolink, Simultaneous determination of carrier lifetime and electron density-of-states in P3HT:PCBM organic solar cells under illumination by impedance spectroscopy, Sol. Energy Mater. Sol. Cells 94 (2010) 366–375, http://dx.doi.org/10.1016/j.solmat.2009.10.015.